Inhibition of ferroptosis reverses heart failure with preserved ejection fraction in mice

Yixiao Xiong[1,2†], Xin Liu[1,2†], Ling Jiang[3,4†], Tao Hao[5], Yanyan Wang[6*] and Tao Li[1,2*]

Abstract

Background Heart failure with preserved ejection fraction (HFpEF) accounts for approximately 50% of heart failure cases. The molecular mechanisms by which HFpEF leads to impaired diastolic function of the heart have not been clarified, nor have the drugs that target the clinical symptoms of HFpEF patients.

Methods HFpEF chip data (GSE180065) was downloaded from the National Center for Biotechnology Information (NCBI) database. Differentially expressed genes (DEGs) were filtered by the limma package in R and processed for GO and KEGG pathway analyses. Then, ferroptosis-related genes in HFpEF were identified by taking the intersection between DEGs and ferroptosis-related genes. CytoHubba and MCODE were used to screen ferroptosis-related hub DEGs in the protein–protein interaction (PPI) network. Establishment of a mouse HFpEF model to validate the transcript levels of ferroptosis-related hub DEGs and ferroptosis-related phenotypes. Transcript levels of ferroptosis-related hub DEGs and HFpEF phenotypic changes in the hearts of HFpEF mice were further examined after the use of ferroptosis inhibitors.

Results GO and KEGG enrichment analyses suggested that the DEGs in HFpEF were significantly enriched in ferroptosis-related pathways. A total of 24 ferroptosis-related DEGs were identified between the ferroptosis gene dataset and the DEGs. The established PPI network was further analyzed by CytoHubba and MCODE modules, and 11 ferroptosis-related hub DEGs in HFpEF were obtained. In animal experiments, HFpEF mice showed significant abnormal activation of ferroptosis. The expression trends of the 11 hub DEGs associated with ferroptosis, except for Cdh1, were consistent with the results of the bioinformatics analysis. Inhibition of ferroptosis alters the transcript levels of 11 ferroptosis-related hub DEGs and ameliorates HFpEF phenotypes.

Conclusions The present study contributes to a deeper understanding of the specific mechanisms by which ferroptosis is involved in the development of HFpEF and suggests that inhibition of ferroptosis may mitigate the progression of HFpEF. In addition, eleven hub genes were recognized as potential drug binding targets.

Keywords Heart failure with preserved ejection fraction, Ferroptosis, Bioinformatics analysis, Ferrostatin-1, Deferiprone

†Yixiao Xiong, Xin Liu and Ling Jiang contributed equally to this work.

*Correspondence:
Yanyan Wang
kittyanwang520@scu.edu.cn
Tao Li
scutaoli1981@scu.edu.cn
Full list of author information is available at the end of the article

Xiong *et al. Journal of Translational Medicine*   (2024) 22:199

Page 2 of 17

Introduction

Heart failure with preserved ejection fraction (HFpEF) is a chronic systemic syndrome characterized by an ejection fraction greater than 50% but with cardiac diastolic dysfunction [1]. Epidemiologic studies have shown that more than half of patients with heart failure have preserved ejection fraction, and this percentage increases over time [2]. Unlike heart failure with reduced ejection fraction (HFrEF), HFpEF is not a disease limited to the heart but involves multiple organs and complications. The prevalence of HFpEF is also increasing with increasing rates of obesity, hypertension and diabetes mellitus [2, 3]. Although the results of a phase III clinical trial showed that empagliflozin (SLGT2 inhibitor) reduced the risk of death due to cardiovascular disease exacerbation in HFpEF patients [4], there is still a lack of evidence-based evidence for the treatment of HFpEF [5]. Therefore, a better understanding of the underlying pathological mechanism is required for the development of new approaches for HFpEF treatment.

Ferroptosis, an oxidized, iron-dependent form of regulated cell death, was first described by Stockwell in 2012 and differs from apoptosis, necrosis and autophagy [6]. This unique programmed cell death is driven by iron-dependent phospholipid peroxidation, which leads to the accumulation of lipid reactive oxygen species (ROS), ultimately leading to cell membrane rupture [7]. Multiple cellular metabolic processes, including iron accumulation, mitochondrial activity, and lipid, amino acid, and carbohydrate metabolism, are involved in the regulation of ferroptosis [8]. Ferroptosis has been implicated in several types of pathological cell death associated with cardiovascular disease (i.e., heart failure, myocardial infarction, cardiomyopathy), cancer, acute renal failure, and other conditions [9–13]. Meanwhile, accumulated evidence has indicated that ferroptosis plays a vital role in the initiation and progression of HFrEF [14, 15], but little evidence shows how it affects HFpEF.

Currently, transcriptomic and microarray analyses have been widely used to identify new biomarkers in HFpEF [16]. In this study, we downloaded a microarray dataset of HFpEF to compare and analyze the original transcriptomic data. We also identified ferroptosis-associated hub genes through intersection with the ferroptosis dataset and protein–protein interaction analysis. Then, we established a HFpEF mouse model and verified the expression of ferroptosis-related hub genes. More importantly, we found that inhibition of ferroptosis significantly alleviated HFpEF-associated clinical phenotypes, such as cardiac diastolic dysfunction and pulmonary congestion, and altered the expression of hub DEGs. These results provide new perspectives on potential therapeutic targets for HFpEF.

Materials and methods

Data information

The microarray profiles in GSE180065 were downloaded from the GEO database. The dataset involves 15 cardiac tissue samples, including 5 control samples, 5 samples with a high-fat diet (HFD)+ Nω-nitro-ʟ-arginine methyl ester (L-NAME, 0.5 g/L dissolved in saline) modeling time of 5 weeks and 5 samples with HFD+L-NAME modeling time of 7 weeks. Five mice modeled with 5 weeks and five control group mice were selected for further bioinformatics analysis. In the original study, the HFpEF model was generated by a combination of a HFD and L-NAME for 5 weeks. The heart tissues were harvested for subsequent experiments.

Differential expression analysis

Data processing was conducted using different packages of R (version: 4.3.0) under RStudio. Briefly, GSE180065_RAW.tar and its corresponding annotation platform GPL24247 were downloaded. The data in the control group and HL5W group were combined in the expression matrix. After normalization, differential expressed genes (DEGs) were identified using the "limma" package. Genes with a p value < 0.05 and $|\log2(\text{fold-change})| \geq 1$ were considered DEGs. The obtained DEGs were then visualized using the R packages "ggplot" and "Heatmap".

Functional enrichment analysis

All DEGs were analyzed by Gene Ontology (GO) and Kyoto Encyclopedia of Genes and Genomes (KEGG) using the enrichGO and enrichKEGG functions in the R package "clusterProfiler".

Identification of ferroptosis-related DEGs

The obtained ferroptosis-related DEGs were uploaded to the STRING online tool. The results were then visualized using Cytoscape to obtain protein–protein interaction (PPI) networks. To obtain the hub genes, the obtained PPI networks were further analyzed using MCODE and CytoHubba plugins in Cytoscape.

Animals

C57BL/6J mice were purchased from Charles River. Mice were placed in an animal house on a 12 h light-dark cycle with unrestricted access to food (normal diet and high-fat diet) and water. L-NAME (0.5 g/l, Sigma-Aldrich) was adjusted to a pH of 7.4 and then added to the drinking water. Ferrostatin-1 (Med Chem Express) was dissolved in 0.1% DMSO and 99.9% corn oil at a concentration of 2 mg ml^{-1} and injected intraperitoneally at a dose of 2 mg kg^{-1} once daily for 2 weeks. Deferiprone (Med Chem

Xiong *et al. Journal of Translational Medicine*   (2024) 22:199

Page 3 of 17

Express) was dissolved in phosphate-buffered saline (PBS) and administered intraperitoneally at 100 mg kg^{-1} over 2 weeks.

Exercise tolerance test

After allowing the mice to acclimatize on the small animal treadmill for 3 weeks, the experimental group of mice was tested for fatigue. The mice were acclimatized to the treadmill with a 20° incline for 4 min starting at a speed of 5 m min^{-1} and increasing by 2 m min^{-1} every two minutes thereafter until the mice were unable to resume running after 10 s of contact with the electrical stimulation grid. The running distance was recorded.

Intraperitoneal glucose tolerance test

After 6 h of fasting, glucose (2 g kg^{-1}) was administered intraperitoneally. Mouse tail blood glucose was measured before (0 min) and 15, 30, 45, 60 and 120 min after intraperitoneal injection.

Conventional echocardiography and Doppler imaging

Echocardiographic measurements were performed under 1.5% isoflurane anesthesia, and the structure and function of the mouse heart were measured using a Vevo 3100 small animal high-resolution sonograph (Fujifilm Visual Sonics), which was swept with an MX550D probe (26–52 MHZ). The heart rate of the mice was maintained at 350–450 beats per minute throughout the ultrasound acquisition. The parameters collected included left ventricular ejection fraction, peak mitral Doppler flow velocity in early diastole, peak mitral Doppler flow velocity in late diastole, and peak tissue Doppler of mitral annular myocardial diastolic velocities in early diastole and early filling deceleration.

Histology

The hearts were rapidly fixed overnight with 4% paraformaldehyde after isolation, embedded in paraffin and sectioned. Staining of heart sections using wheat germ agglutinin (WGA) and Masson's trichrome (MT). Immunochemical staining of myocardial sections was performed using a CD31 primary antibody (1:2000, Cat. ab182981, Abcam). WGA results were observed using an Olympus IX83 microscope and quantitatively analyzed using ImageJ software 2.0. MT-stained and CD31 immunohistochemically stained sections were observed using a ZEISS Imager. A2 microscope. Tissue Prussian blue staining was performed using a Prussian blue staining kit (Cat. G1422, Solarbio) and observed using a ZEISS Imager. A2 microscope.

IHC analysis

Heart myocardial tissues were isolated and fixed with 4% paraformaldehyde. After routine paraffin-embedded sections, the sections were deparaffinized and immersed in antigen repair solution and microwaved for 8 min, repeated three times. After cooling in a ventilated area, the slides were blocked by 5% bovine serum albumin (BSA) for 1 h and again washed 3 times with TBST. The slides were treated with 0.1% Triton X-100 for 10 min and then washed three times with TBST. Then the sections were incubated with F4/80 Polyclonal antibody (1:4000, Cat. 28463-1-AP, Proteintech) overnight. After incubation, slides were washed 3 times with TBST and incubated with goat anti-rabbit IgG (Alexa Fluor 594, 1:500; ab150080, Abcam) for 30 min at room temperature. The slides were washed 3 times with TBST and the slides were incubated with 4',6-diamidino-2-phenylindole (DAPI). Images were visualized using a ZEISS Imager. A2 microscope microscope system and processed with ZEISS software.

Measurement of ROS

To assess ROS production, the heart was carefully and quickly isolated, cut into 4.0 μm sections and placed on chilled microscope slides. The samples were incubated in physiological saline containing 10 μmol dihydroethidium (DHE; Cat. 104821-25-2, Sigma-Aldrich) for 30 min at 37 °C in the dark. The heart sections were washed twice with PBS and placed under an automatic fluorescence microscope (BX63, Olympus).

Transmission electron microscopy (TEM)

2-mm × 2-mm × 2-mm pieces were removed from the apical region of freshly isolated mouse hearts and immediately fixed in 2.5% glutaraldehyde overnight. After embedding and cutting, they were observed under FEI Tecnai Spirit 120-kV TEM.

Total iron ion content measurement

Hearts were isolated from mice, 0.1 g of fresh myocardium was taken from the septal region of freshly isolated hearts, and the iron ion content was determined using a total iron ion colorimetric test kit (Cat. E-BC-K772-M, Elabscience).

Superoxide dismutase (SOD) activity level measurement

Hearts were isolated from mice, 0.1 g of fresh myocardial tissue was homogenized with magnetic beads at 4 °C and centrifuged at 4 °C, and the supernatants were removed. The level of SOD activity in the supernatant

was assayed using a total SOD activity assay kit (Cat. S0109, Beyotime).

Malondialdehyde (MDA) level measurement

Myocardial tissue was homogenized using precooled PBS, and the supernatant was centrifuged at 4 °C. The MDA content of the supernatant and plasma was determined using a malondialdehyde assay kit (Cat. S0131S, Beyotime).

Western blot analysis

Tissues or cultured cells were lysed in RIPA buffer containing a protease inhibitor cocktail (Roche) for 30 min on ice. Protein (10–20 μg) was separated by SDS-PAGE. Western blotting was performed with NRF2 (1:2000, Cat. 16396-1-AP, Proteintech), ATF4 (1:500, Cat.10835-1-AP, Proteintech), SLC7A11 (1:2000, Car.26864-1-AP, Proteintech), GPX4 (1:1000, Cat. 67763-1-Ig, Proteintech) and GAPDH (1:10000, Cat. 60004-1-Ig, Proteintech) antibodies. The band intensities of target proteins were analyzed by using the ImageJ software.

RT-qPCR

Mouse heart tissue was lysed using TRIzol reagent (Ambion), and total RNA was extracted. Total RNA was reverse transcribed using a reverse transcription kit (Bio-Rad). qPCR experiments were performed using a SYBR mixture (Bio-Rad). GAPDH was used to normalize and calculate fold ratios relative to the mRNA expression level of control samples. The PCR primer sequences used are shown in Additional file 1: Table S1.

Statistical analysis

Data were statistically analyzed using GraphPad Prism 9.0 and then plotted on graphs and expressed as the mean ± SEM. The normality of the data was tested. Comparisons between two groups were performed using a two-tailed Student's t-test with a 95% confidence interval. Comparisons for > 2 groups were analyzed using a one-way or two-way ANOVA followed by Bonferroni post hoc analysis. $P < 0.05$ was considered statistically significant.

Results

DEGs in HFpEF and functional enrichment analysis

The microarray expression profiling dataset GSE180065 was obtained from the GEO database. Compared with controls, 952 differentially expressed genes were identified by differential analysis in HFpEF mouse heart samples, including 483 upregulated genes and 469 downregulated genes (Additional file 2: Table S2). A volcano plot was used to visualize the DEGs (Fig. 1A). The top

100 DEGs in the dataset were clustered and are shown in the form of a heatmap (Fig. 1B).

GO and KEGG analyses were used to further identify the major functions and pathways associated with the DEGs. The GO terms were categorized as biological processes (BP), cellular components (CC), and molecular functions (MF). For BP, four of the top ten GO terms are closely related to ferroptosis, including regulation of inflammatory response, response to metal ion, ROS metabolic process and negative regulation of cell activation. A chordal map was used to visualize the top five KEGG-enriched pathways, including the peroxisome proliferator-activated receptor (PPAR) signaling pathway, cholesterol metabolism, apelin signaling pathway, cytokine–cytokine receptor interaction and Cushing syndrome (Additional file 3: Fig. S1A). KEGG enrichment analysis indicated that the DEGs are mainly involved in the PPAR signaling pathway. The PPAR signaling pathway is thought to be closely related to ferroptosis [17, 18]. Although the ferroptosis pathway was not directly enriched in the analysis of HFpEF mouse samples, both GO and KEGG results clearly demonstrated that the ferroptosis-related metabolic pathway was significantly enriched in the hearts of HFpEF mice. Specific GO and KEGG analysis results are shown in the supplementary material (Additional file 4: Table S3, Additional file 5: Table S4).

Ferroptosis-related hub DEGs in HFpEF mice

To further explore the potential mechanism of ferroptosis in HFpEF, we downloaded a dataset containing 844 genes from FerrDb and intersected them with DEGs in GSE180065 to identify ferroptosis-related genes. As shown by the Venn diagram, a total of 24 genes were obtained from the intersection of DEGs and ferroptosis-related genes, including 15 upregulated and 9 downregulated genes (Fig. 2A). DEGs in the intersection set were further categorized into ferroptosis drivers, ferroptosis suppressors, and unclassified via FerrDb (Table 1). We then analyzed GO and KEGG enrichment for these 24 ferroptosis-related DEGs and displayed the top five terms of BP, CC and MF as bubble plots and the top five KEGG enrichments as chord plots (Fig. 2B, C). All results of functional and pathway enrichment analyses on ferroptosis-related genes are shown in the supplementary material (Additional file 6: Table S5, Additional file 7: Table S6). In the BP part, functional analysis was mainly enriched in pathways such as neuron death and cellular response to metal ions. It is worth noting that the PPAR signaling pathway ranked in the top 5 in both KEGG analyses. Then, the PPI of the 24 ferroptosis-related DEGs was analyzed using the STRING online tool and visualized as a network by Cytoscape, including 18 nodes and 48 edges (Fig. 2D). Six
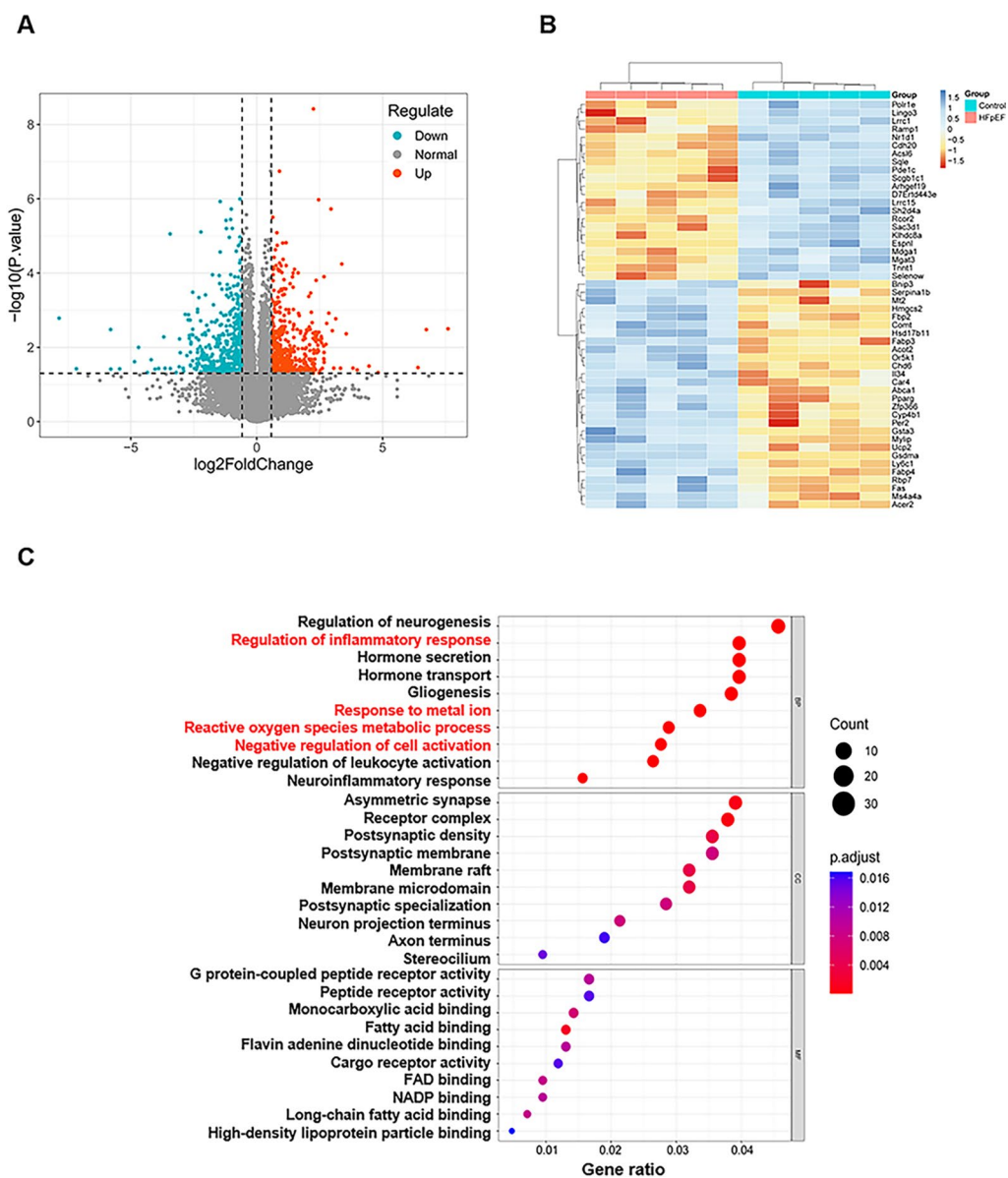
Xiong *et al. Journal of Translational Medicine*　　(2024) 22:199

Page 5 of 17

Fig. 1 DEGs in HFpEF and results of GO and KEGG analysis. **A** Volcano plot of DEGs in GSE180065. **B** Clustered heatmap of the first 50 DEGs in GSE180065. **C** The enriched GO terms of DEGs in GSE180065

genes were not related to other molecules. The MCODE plugin in Cytoscape was used to identify gene clusters in the ferroptosis hub DEGs. After filtering criteria were set to degree cutoff = 2, node score cutoff = 0.2, k hub = 2 and max depth = 100, a module with 11 nodes and 36 edges was identified with genes including *Lcn2, Hmox1, Il1b, Tlr4, Pparg, Egr1, Tfap2a, Creb1, Vdr, Cdh1,* and *Cd44* (Fig. 2E). We analyzed the PPI network again using the MCC algorithm in the plugin CytoHubba and screened 10 candidate hub DEGs, including *Cd44, Egr1, Cdh1, Pparg, Il1b, Tlr4, Hmox1, Vdr, Creb1,* and *Lcn2* (Fig. 2F). Combining these

two results, we obtained 11 hub ferroptosis-related genes, including *Lcn2, Hmox1, Il1b, Tlr4, Pparg, Egr1, Tfap2a, Creb1, Vdr, Cdh1,* and *Cd44*. Seven of the upregulated genes included *Lcn2, Hmox1, Il1b, Pparg, Tlr4, Cd44,* and *Creb1*, and four downregulated genes included *Vdr, Cdh1, Egr1,* and *Tfap2a*.

Validation of ferroptosis-related hub DEGs expression in HFpEF mice

We first established a mouse model of HFpEF according to previous methods by inducing a distinct HFpEF
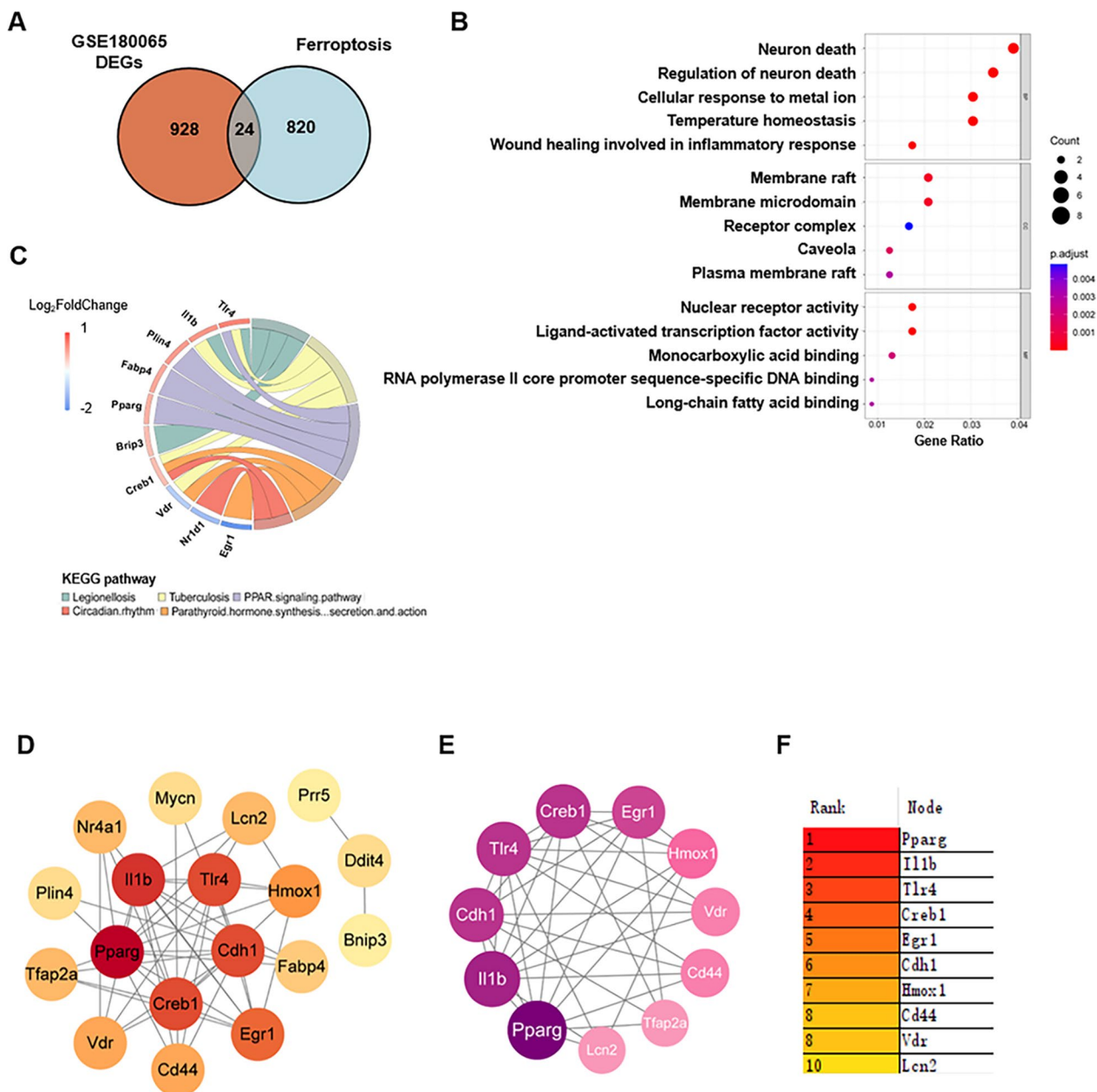
Fig. 2 Identification of ferroptosis-related hub DEGs in HFpEF mice. **A** Venn plot of hub genes in the DEGs and FerrDb. **B** The enriched GO terms of ferroptosis-related DEGs. **C** KEGG pathway enrichment results for ferroptosis-related DEGs. **D** PPI network of ferroptosis-related DEGs. **E** A key cluster with 11 genes was further chosen as hub genes by MCODE. **F** Top 10 hub genes explored by CytoHubba

Table 1 The ferroptosis-related DEGs were divided into ferroptosis driver, suppressor, and unclassified

Drive	Suppressor	Unclassified
Egr1, Hmox1, Il1β	Acot1, Cd44, Cdh1	Binp3, Ddit4, Hsd17b1
Pparg, Tlr4, Nr1d1	Fabp4, Lcn2, Nr4a1	Lurap1l, Plin4, Rgs4
Mycn, Ttpa	Tfap2a, Vdr, Creb1	
	Prr5	

phenotype in mice with HFD+L-NAME for 5 weeks [19]. The left ventricular ejection fraction (LVEF) remained unchanged in HFD– and L-NAME-fed mice compared with regular diet-fed mice (Fig. 3A, B). However, increased E/A ratio and E/e′ ratio indicate significant diastolic dysfunction in HFpEF mice. The increased left ventricular posterior wall thickness at diastole (LVPWd), left ventricular internal diameter at diastole (LVDd),

left ventricular internal diameter at systole (LVDs) and interventricular septal end diastole (LVSd) also simultaneously demonstrated both increased stress loading and decreased diastolic function in HFpEF mice. (Fig. 3C–F and Additional file 8: Fig. S2A–D). HFD+L-NAME feeding also significantly induced weight gain, decreased exercise tolerance, and impaired glucose tolerance in mice (Fig. 3G–I and Additional file 8: Fig. S2E). We then found that HFpEF mice demonstrated significant cardiac enlargement and pulmonary congestion (Fig. 3J, K). The decline in cardiac function in HFpEF mice was also accompanied by a significant increase in the mRNA expression levels of *Bnp* and genes related to myocardial fibrosis, such as *α-SMA*, *Fn1*, *Col1a2*, and *Timp1* (Fig. 3L, M). At the same time, histologic findings also suggested that HFD+L-NAME led to cardiomyocyte enlargement, myocardial fibrosis, and a reduction in capillary density (Fig. 3N–S). To verify whether HFpEF mice showed overactivation of the immune system, we examined macrophage infiltration in the myocardium of HFpEF mice. The immunofluorescence results suggested significant macrophage recruitment in the myocardium of HFpEF mice (Additional file 8: Fig. S2F). Then, RT-qPCR was used to verify the transcript levels of previously screened genes associated with ferroptosis in the hearts of HFpEF mice. Compared to the control group, *Lcn2*, *Hmox1*, *Il1b*, *Pparg*, *Tlr4*, *Cd44*, and *Creb1* had significantly increased transcript levels in the HFpEF group (P < 0.05), while *Vdr*, *Egr1* and *Tfap2a* exhibited markedly decreased expression in the HFpEF group (P < 0.05). However, there was no significant difference in *Cdh1* expression between the HFpEF and control groups (Fig. 3T).

Ferroptosis is activated in HFpEF

Recent studies have shown that ferroptosis plays an important role in heart failure, while the pathogenesis of ferroptosis involved in HFpEF has not been elucidated [20, 21]. To determine the abnormal activation of ferroptosis in HFD+L-NAME-induced HFpEF mice and the

potential mechanism behind it, we analyzed the mRNA expression of *Ptgs2*, a biochemical marker of ferroptosis [22]. As expected, *Ptgs2* mRNA was significantly upregulated more than in the hearts of HFpEF mice (Fig. 4A). Ferroptosis is mainly realized as intracellular iron overload, which further leads to lipid peroxidation [23]. We first stained the myocardial tissue with Prussian blue and measured the iron ion content in the myocardial tissue. Compared with the control group, we found that the percentage of trivalent iron-containing cells in the myocardial tissue of HFpEF mice was significantly increased and that the total iron content was significantly higher than that in control mice (Fig. 4B, C).

Excess iron promotes the production of mitochondrial ROS through the Fenton reaction, and mitochondrial ROS undergo lipid peroxidation due to the reaction of polyunsaturated fatty acids on the mitochondrial membrane [24, 25]. SOD is an enzyme that converts superoxide, such as ROS, into less damaging hydrogen peroxide. Compared with control mice, HFpEF mice showed an increase in ROS content in myocardial tissue and a significant decrease in SOD activity (Fig. 4D, E). Transmission electron microscopy was used to examine mitochondrial morphology. As expected, we found ultrastructural changes with ferroptosis features such as reduction in mitochondrial volume, increase in mitochondrial membrane density, and disappearance of mitochondrial cristaein the hearts of HFpEF mice (Fig. 4F). We further examined the level of MDA, a biomarker of lipid peroxidation and a critical indicator of ferroptosis in vivo, in the plasma and heart tissues of mice [23]. We found that MDA levels in plasma and myocardial tissue were significantly higher in HFpEF mice than in control mice (Fig. 4G, H). In addition to iron overload, loss of glutathione (GSH) is another key mechanism of ferroptosis, and intracellular GSH production requires SLC7A11, which transports cystine (a precursor of GSH) into the cytoplasm [26]. At the same time, inactivation of glutathione peroxidase 4 (Gpx4) also leads to loss of

(See figure on next page.)

Fig. 3 Validation of ferroptosis-associated hub DEGs expression in the hearts of HFpEF mice. **A–T** Control mice and HFpEF mice were both fed a normal diet (Control) or HFD+L-NAME (HFpEF) for 5 weeks. **A** Representative left ventricular M-mode echocardiographic tracings. **B** Percentage of LVEF, n = 5 mice per group. **C, D** Representative pulsed-wave and tissue Doppler tracings, n = 5 mice per group. **D–F** Percentage of ratio between mitral E wave and A wave; ratio between mitral E wave and e′ wave (E/e′); n = 5 mice per group. **G** Body weights of the two groups of mice after 5 weeks of rearing, n = 5 mice per group. **H** Running distances of the two groups of mice during the exercise tolerance test, n = 5 mice per group. **I** Mouse tail blood glucose at different time points in the intraperitoneal glucose tolerance test, n = 5 mice per group. **J** Ratio between wet and dry lung weight, n = 5 mice per group. **K** Ratio between heart weight and tibia length, n = 5 mice per group. **L, M** mRNA levels of *Bnp* and myocardial fibrosis-related genes (*a-SMA, Fn1, Col1a2, Timp1*) in myocardial tissues of mice in the two groups, n = 5 mice per group. **N–P** Representative images of WGA, MT and CD31-stained heart sections from control and HFpEF mice. **Q** WGA quantification of cardiomyocyte cross-sectional area, n = 5 mice per group (scale bar: 50 μm). **R** Percentage of fibrosis area in MT-stained heart sections, n = 5 mice per group (scale bar: 50 μm). **S** Myocardial capillary density, n = 5 mice per group (scale bar: 50 μm). **T** Ferroptosis-associated hub DEG mRNA expression in control and HFpEF mice. Statistical significance was calculated by Student's t test; *P < 0.05, **P < 0.01, and ***P < 0.001
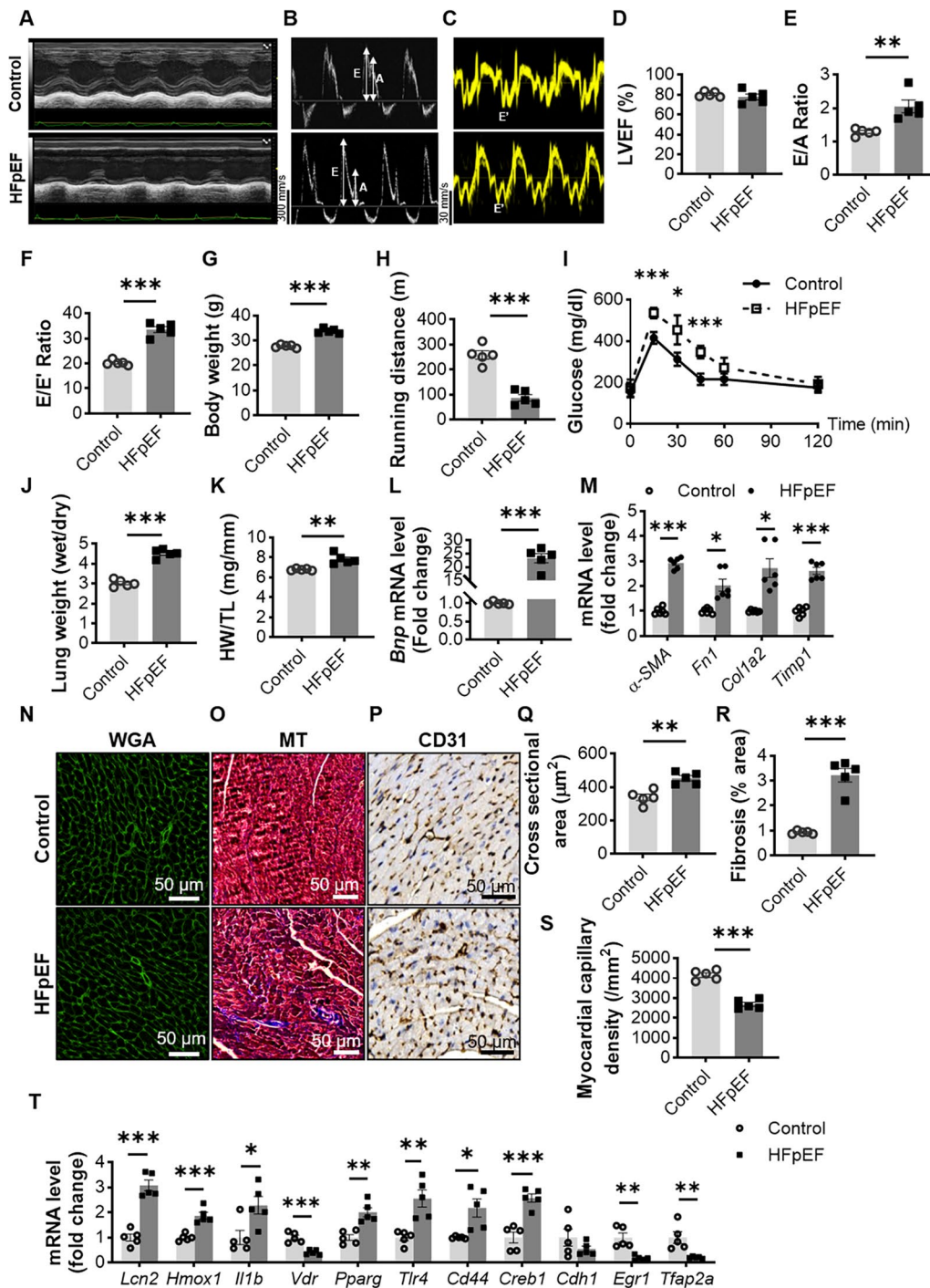
Fig. 3 (See legend on previous page.)

GSH and activation of ferroptosis [27]. We found that the protein levels of SLC7A11 and GPX4 in the myocardial tissue of HFpEF mice were significantly reduced (Fig. 4I). Nuclear factor red lineage 2-related factor 2 (NRF2) and activating transcription factor 4 (ATF4) can directly or indirectly regulate GPX4 activity [28, 29]. We then examined the protein expression levels of ATF4 and NRF2 in the myocardial tissues of the mice, and we found that there was no significant change in the levels of ATF4 in the myocardium of the HFpEF mice, but NRF2 appeared to be significantly reduced (Fig. 4I). These results suggest that HFD and circulating high load
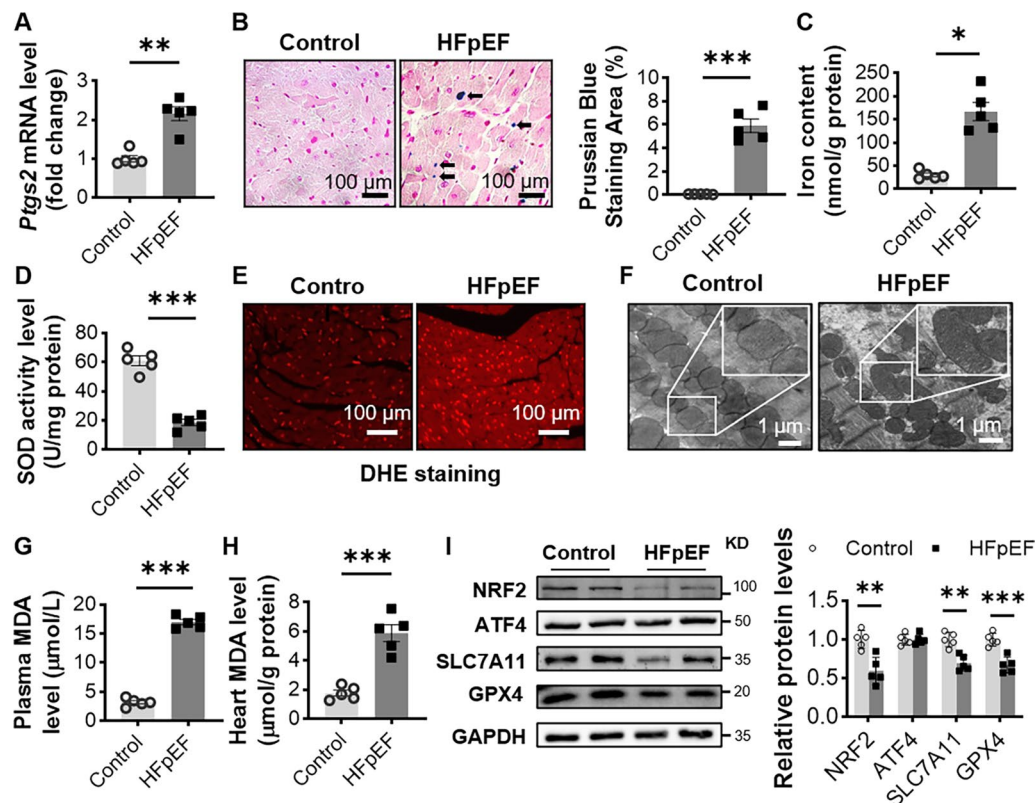
Xiong *et al. Journal of Translational Medicine* (2024) 22:199

Page 9 of 17

Fig. 4 HFpEF mouse hearts showed abnormal activation of ferroptosis. **A** Relative expression of *Ptgs2* mRNA in myocardial tissues using RT-qPCR. *Gapdh* was used as an internal reference, n = 5 mice per group. **B** Representative Prussian blue-stained images of cross-sections of two groups of mouse hearts, and black arrows show blue-stained cardiomyocytes; Percentage of Prussian blue-stained positive cells, n = 5 mice per group. **C** Measurement of total iron ion content in myocardial tissue, n = 5 mice per group. **D** SOD activity level in myocardial tissue, n = 5 mice per group. **E** Representative DHE staining images of heart tissue, n = 5 mice per group. **F** Representative transmission electron microscopy images of heart tissue, n = 5 mice per group. **G**, **H** MDA levels in plasma and heart tissue, n = 5 mice per group. **I** Representative western blot images and average protein levels of SLC7A11, GPX4, NRF2 and ATF4 in control and HFpEF mouse hearts, n = 5 mice per group. Statistical significance was calculated by Student's t test; *$P < 0.05$, **$P < 0.01$, and ***$P < 0.001$

(L-NAME-induced) may regulate GPX4 activity through NRF2 and thus cause ferroptosis.

Ferrostatin-1 inhibits ferroptosis and alters the transcript levels of ferroptosis hub DEGs

To investigate whether ferroptosis is involved in the development of HFpEF, we used two ferroptosis inhibitors, Ferrostatin-1 (Fer-1) and deferiprone (DFP). Fer-1 directly inhibits lipid peroxidation, whereas DFP acts as an iron specific chelator and is used in the clinical treatment of iron overload diseases [28, 30]. We divided HFD+L-NAME-fed mice for 5 weeks into three groups, one receiving intraperitoneal Fer-1 for 2 weeks, one receiving intraperitoneal DFP for 2 weeks and the other receiving intraperitoneal injection of vehicle for 2 weeks (Fig. 5A). First, we found that the *Ptgs2* mRNA expression levels were significantly reduced in the myocardial tissue of the HFpEF+Fer-1 and HFpEF+DFP group (Fig. 5B). Meanwhile, the number of trivalent

iron-containing cells in the myocardial tissue of mice was significantly reduced, and the total iron content were also significantly lower after Fer-1 or DFP injection (Fig. 5C, D and Additional file 9: Fig. S3A). For HFpEF mice injected intraperitoneally with Fer-1 or DFP, a significant increase in myocardial tissue SOD activity was accompanied by a significant decrease in ROS (Fig. 5E, F). Transmission electron microscopy results also suggested that Fer-1 and DFP prevented mitochondrial deformation caused by HFD+L-NAME (Fig. 5G). We also found a significant decrease in MDA levels in the heart and blood after intraperitoneal injection of Fer-1 or DFP (Fig. 5H, I). The western blot results suggested that compared with HFpEF+Veh mice, the myocardial tissues of HFpEF+Fer-1 and HFpEF+DFP mice showed a significant increase in the levels of SLC7A11 and GPX4 protein expression, as well as a significant increase in the expression of NRF2, which directly regulates the activity of GPX4, but there was no difference in the content of ATF4
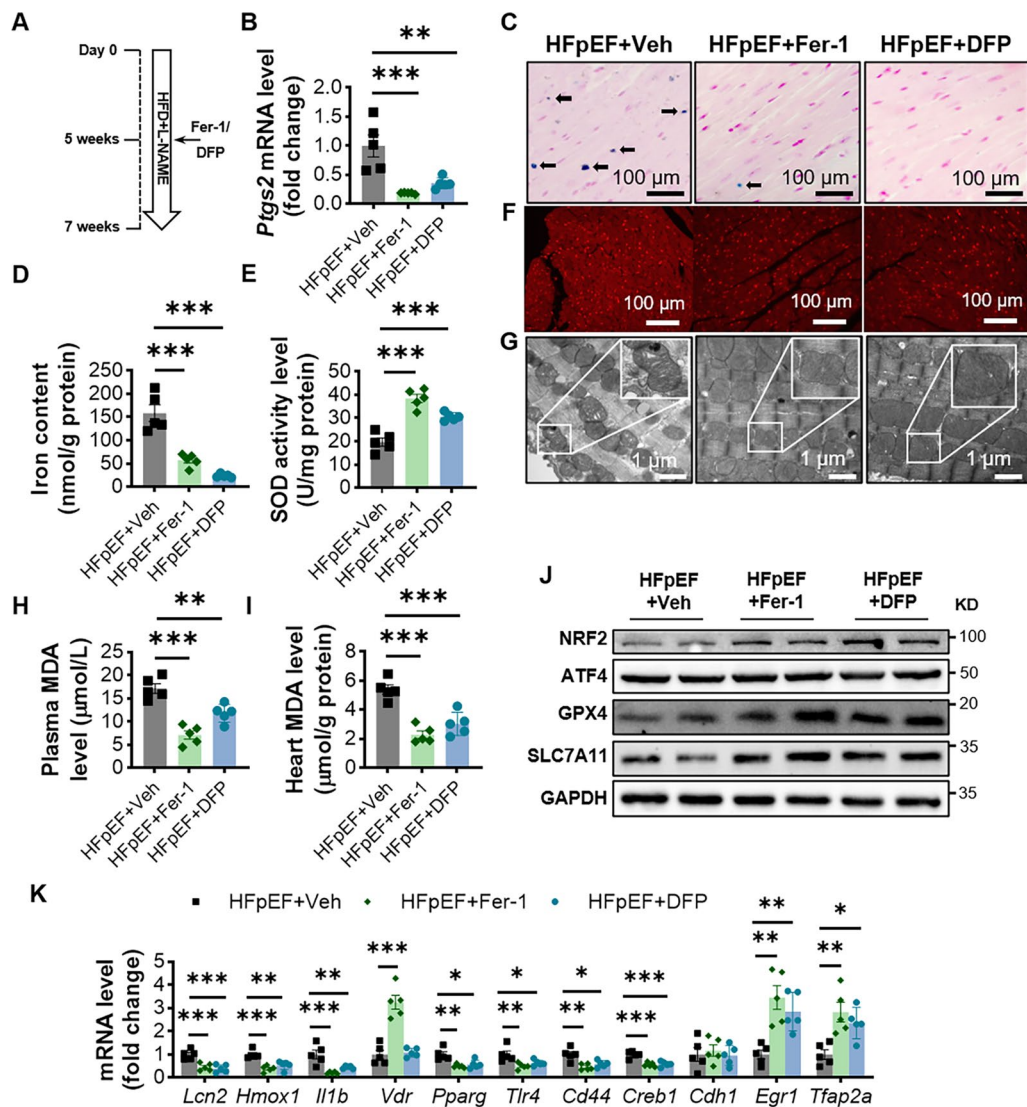
Xiong *et al. Journal of Translational Medicine* (2024) 22:199

Page 10 of 17

Fig. 5 Ferrostatin-1 inhibits ferroptosis and alters the expression levels of ferroptosis hub DEGs. **A** Experimental design. **B** Relative expression of *Ptgs2* mRNA in myocardial tissues using RT-qPCR. *Gapdh* was used as an internal reference, n = 5 mice per group. **C** Representative Prussian blue-stained images of cross-sections of two groups of mouse hearts, and black arrows show blue-stained cardiomyocytes; Percentage of Prussian blue-stained positive cells, n = 5 mice per group. **D** Measurement of total iron ion content in myocardial tissue, n = 5 mice per group. **E** SOD activity level in myocardial tissue, n = 5 mice per group. **F** Representative DHE staining images of heart tissue, n = 5 mice per group. **G** Representative transmission electron microscopy images of cardiac tissue, n = 5 mice per group. **H, I** MDA levels in plasma and heart tissue, n = 5 mice per group. **J** Representative western blot images and average protein levels of SLC7A11, GPX4, NRF2 and ATF4 in HFpEF+Veh, HFpEF+Fer-1 and HFpEF+DFP mouse hearts, n = 5 mice per group. **K** Ferroptosis-associated hub DEGs mRNA expression in HFpEF+Veh and HFpEF+Fer-1 mice. Statistical significance was calculated by one-way or two-way ANOVA; *P < 0.05, **P < 0.01, and ***P < 0.001

(Fig. 5J and Additional file 9: Fig. S3B). Together, these results suggest that Fer-1 and DFP inhibit ferroptosis in the hearts of HFpEF mice.

Then, we examined the expression levels of ferroptosis hub DEGs after intraperitoneal injection of Fer-1 or DFP. The results indicated that the transcript levels of *Lcn2*, *Hmox1*, *Il1b*, *Pparg*, *Tlr4*, *Cd44* and *Creb1* in the hearts of mice in the Fer-1 or DFP group were

significantly lower than those in the vehicle group, and the transcript levels of *Egr1* and *Tfap2a* were significantly higher than those in the HFpEF+Veh group (Fig. 5K). For HFpEF mice, intraperitoneal injection of Fer-1 but not DFP increases *Vdr* expression levels in myocardial tissue. However, we did not find significant differences in *Cdh1* mRNA expression among the three groups of mice (Fig. 5K).

Xiong *et al. Journal of Translational Medicine*   (2024) 22:199

Page 11 of 17

The HFpEF phenotype is ameliorated by inhibition of ferroptosis

We further examined the HFpEF-related phenotypes in three groups of mice to determine whether attenuating ferroptosis could mitigate the progression of HFpEF. As shown in the echocardiograms, although the left ventricular ejection fraction did not change much in either group, the E/A ratio, E/e′ ratio, LVPWd, LVDd, LVDs and LVSd of the mice in the HFpEF+Fer-1 and HFpEF+DFP groups were significantly lower than those in the HFpEF+Veh group, indicating that the diastolic function of the heart was significantly improved (Fig. 6A–F and Additional file 9: Fig. S3C–F). Intraperitoneal injection of Fer-1 did not significantly reduce HFpEF body weight, but DFP did reduce body weight in mice (Fig. 6G). Exercise tolerance and glucose tolerance were significantly higher in the HFpEF+Fer-1 group than in the HFpEF+Veh group, but there was no significant difference in the HFpEF+DFP group (Fig. 6H, I and Additional file 8: Fig. S2G). Meanwhile, inhibition of ferroptosis in HFpEF mice demonstrated robust reductions in heart size and lung weight compared with those in the HFpEF+Veh group, suggesting significant remission of pulmonary congestion and preclinical heart failure states (Fig. 6J, K). The RT-qPCR results indicated that the transcript levels of myocardial fibrosis-related genes and *Bnp* were significantly reduced in the Fer-1 or DFP treatment group (Fig. 6L, M). The HFpEF+Veh group showed marked cardiomyocyte hypertrophy, cardiac fibrosis and reduced myocardial capillary density, which were markedly ameliorated by inhibition of ferroptosis (Fig. 6N–S). Fer-1 and DFP also significantly reduced macrophage infiltration within the myocardial tissue of HFpEF mice (Additional file 9: Fig. S3H). The above results prove that inhibition of abnormally activated ferroptosis in HFpEF mice significantly ameliorated HFpEF-related phenotypes such as diastolic dysfunction of the heart and pulmonary congestion in HFpEF mice.

Discussion

Our study uncovered for the first time the key genes associated with ferroptosis in HFpEF disease, and based on this, we further explored the potential mechanism of action of ferroptosis in HFpEF. We obtained 24 DEGs, including 15 upregulated genes and 9 downregulated genes, by analyzing the GSE180065 dataset downloaded from the NCBI database and intersecting the DEGs with the gene set downloaded from FerrDB. The STRING online tool and the MCODE and CytoHubba plugins in Cytoscape were then used to screen 11 ferroptosis-related hub DEGs. Abnormal activation of ferroptosis was found in mice constructed with the HFpEF phenotype using the 'two hit' model, and changes in the expression level of ferroptosis-associated hub DEGs were determined using RT-qPCR. After intraperitoneal injection of Ferrostatin-1, the expression of ferroptosis-related core genes in the hearts of HFpEF mice was identified, while results such as cardiac ultrasound and pathology suggested that inhibition of the ferroptosis pathway could significantly improve the HFpEF phenotype.

Previous studies have shown that HFpEF, as a distinct and prevalent form of heart failure, is significantly associated with metabolic syndrome. Increased visceral fat due to obesity, dyslipidemia, type 2 diabetes mellitus and hypertension associated with a high-salt diet serves as an important risk factor for HFpEF [31]. From another perspective, the major role played by visceral adipose tissue in the development of HFpEF also suggests that the pathogenesis of HFpEF is inextricably linked to systemic metabolic disturbances [32, 33]. Metabolic syndrome puts the body in a chronic inflammatory state for a long time, and the imbalance of oxidative stress and antioxidants in the body further causes abnormal accumulation of ROS, microvascular injury, compensatory hypertrophy of cardiomyocytes and myocardial fibrosis, and finally develops into diastolic dysfunction and even HFrEF [34]. Meanwhile, the pathogenesis of ferroptosis in heart failure, which is mainly characterized by iron overload and lipid peroxidation, has been gradually elucidated,

(See figure on next page.)

Fig. 6 Inhibition of ferroptosis alleviates HFpEF. **A** Representative left ventricular M-mode echocardiographic tracings. **B** Representative pulsed-wave Doppler tracings. **C** Representative tissue Doppler tracings. **D–F** Percentage of LVEF; ratio between mitral E wave and A wave; ratio between mitral E wave and e′ wave (E/e′); n = 5 mice per group. **G** Body weights of the two groups of mice after 7 weeks of rearing, n = 5 mice per group. **H** Running distances of the two groups of mice during the exercise tolerance test, n = 5 mice per group. **I** Mouse tail blood glucose at different time points in the intraperitoneal glucose tolerance test, n = 5 mice per group. *Indicates the comparison between the HFpEF+Veh and HFpEF+Fer-1 group; #indicates the comparison between the HFpEF+Veh and HFpEF+DFP group. **J** Ratio between wet and dry lung weight, n = 5 mice per group. **K** Ratio between heart weight and tibia length, n = 5 mice per group. **L, M** mRNA levels of *Bnp* and myocardial fibrosis-related genes (*a-SMA*, *Fn1*, *Col1a2*, *Timp1*) in myocardial tissues of mice in the two groups, n = 5 mice per group. **N–P** Representative images of WGA, MT and CD31-stained heart sections from the two groups of mice. **Q** WGA quantification of cardiomyocyte cross-sectional area, n = 5 mice per group (scale bar: 50 μm). **R** Percentage of fibrosis area in MT-stained heart sections, n = 5 mice per group (scale bar: 50 μm). **S** Myocardial capillary density, n = 5 mice per group (scale bar: 50 μm). Statistical significance was calculated by one-way or two-way ANOVA; *P < 0.05, **P < 0.01, and ***P < 0.001
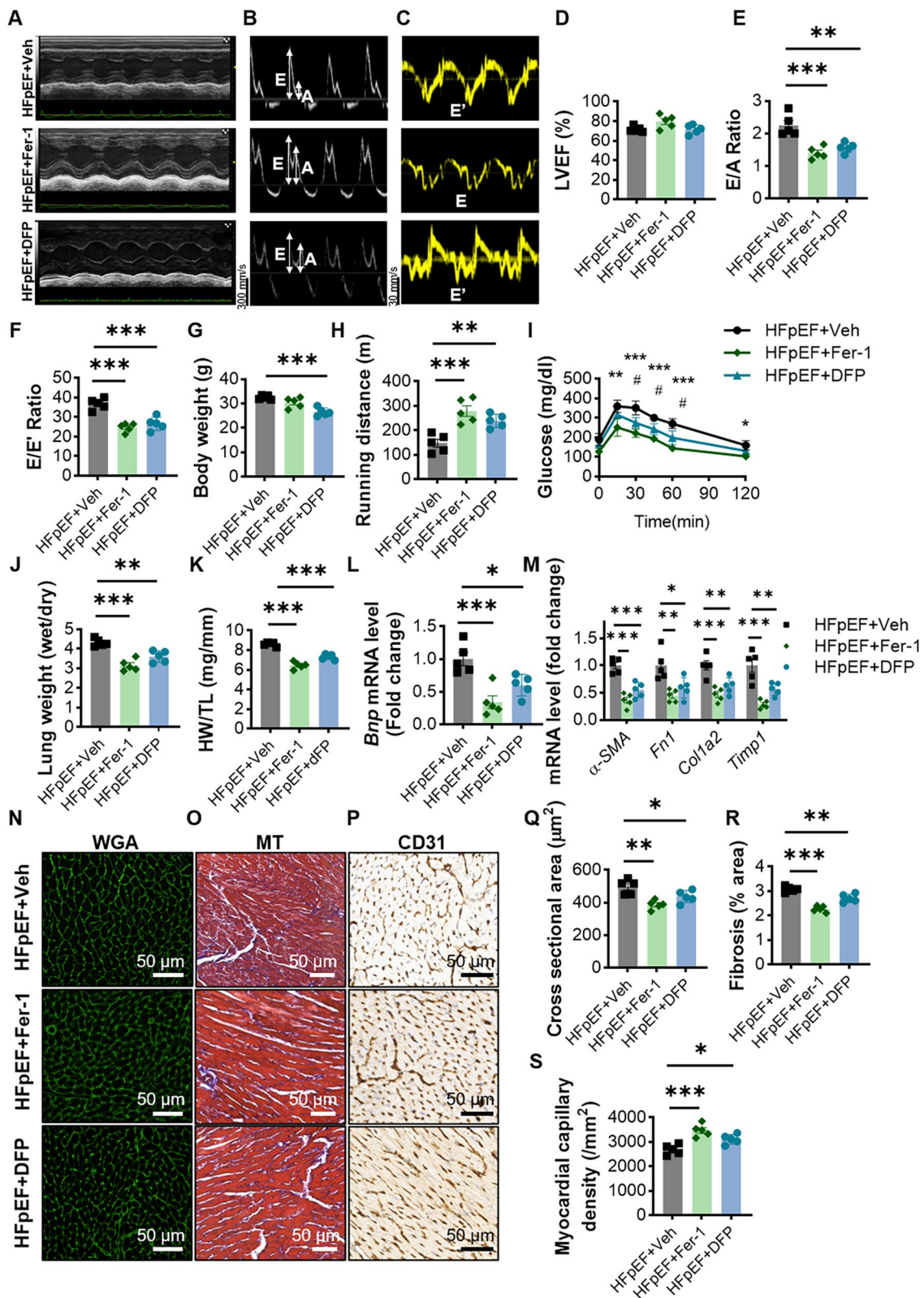
Fig. 6 (See legend on previous page.)

Xiong *et al. Journal of Translational Medicine*   (2024) 22:199

Page 13 of 17

suggesting the potential pathogenesis of HFpEF [25, 35]. Previous studies have shown that when ferroptosis is increased, the immune system is reactively activated and involved in regulating the immune response [36–38]. Patients with HFpEF exhibit higher levels of inflammation and increased inflammatory factors in the somatic circulation, leading to endothelial cell injury [39, 40]. Damaged endothelial cells accumulate in the microcirculation through endothelial cell adhesion molecules and e-selectin, which recruit immune cells, especially macrophages, to the microcirculation, further leading to microcirculatory blockage, and inflammatory factors secreted by immune cells, such as Il-1b, Il-6, and TNF-a, in turn activate the inflammatory system, leading to a vicious cycle [41–44].

However, no study has examined the independent role of ferroptosis in HFpEF. Therefore, in this study, we attempted to explore the association between ferroptosis and HFpEF through bioinformatics analysis combined with experimental validation. The results obtained from our functional and pathway enrichment analysis of 952 DEGs suggest a major enrichment in immunoinflammatory pathways, such as regulation of inflammatory response, response to metal ion, ROS metabolic process, PPAR signaling pathway, negative regulation of cell activation and negative regulation of leukocyte activation, suggesting that the development of HFpEF is indeed related to immune and inflammatory interactions. Then, a total of 24 DEGs overlapping in ferroptosis and HFpEF were identified in this study. We analyzed the obtained ferroptosis-related DEGs for functional and pathway enrichment. Interestingly, both enrichment analyses enriched the PPAR signaling pathway, monocarboxylic acid binding and long-chain fatty acid binding. The PPAR signaling pathway is closely related to fatty acid metabolism and immunoregulation [45]. The involvement of the PPAR signaling pathway in HFpEF does not appear to have been fully elucidated. A report found that SIRT6 in rat vascular endothelial cells improves cardiac diastolic function by inhibiting PPARγ expression in endothelial cells [46], while another article suggested that PPARγ activation may reduce systolic blood pressure and left ventricular mass and attenuate myocardial fibrosis in HFpEF rats by inhibiting the Wnt-β-catenin pathway [47]. All of this evidence suggests that activation of the PPAR signaling pathway plays a role in the development of HFpEF, but further experimental validation is still needed.

Then, we screened ferroptosis-related DEGs in GSE180065 by MCODE and CytoHubba plugins in Cytoscape and obtained 11 hub DEGs. *Pparg*, the top-ranked hub DEGs by CytoHubba, encodes the PPAR receptor γ subtype [48]. *Pparg* is predominantly

expressed in adipose tissue and plays a key role in lipid metabolism and the maintenance of energy homeostasis [48, 49]. For the heart, an organ that primarily utilizes fatty acids, *Pparg* deficiency leads to ventricular contractile dysfunction and intracellular fatty acid overload in cardiomyocytes in mice, whereas pioglitazone, an agonist of *Pparg*, reverses hypoxia-induced pulmonary hypertension and ventricular remodeling in rats [50]. Similarly, our results also confirmed that the transcriptional level of *Pparg* was significantly upregulated in the hearts of HFpEF mice and that the ferroptosis inhibitor Ferrostatin-1 downregulated its expression. *Il1b* encodes a protein that is a cytokine produced primarily by activated macrophages and is involved in the immune response and assembly of inflammatory vesicles such as NLRP3 [51]. Studies have shown that the assembly of NLRP3 inflammatory vesicles can further cause ferroptosis [52]. In addition, NLRP3 inflammatory vesicles have been shown to be closely associated with cardiac inflammation and myocardial hypertrophy [43, 53]. *Tlr4* encodes Toll-like receptor 4 protein, which is involved in immune responses such as pathogen recognition and immune activation. Toll-like receptor 4 activation by LPS can activate the NF-κB pathway, which leads to increased HIF-1a expression, further causing ferroptosis [54]. Meanwhile, the NF-κB pathway and the JAK/STAT3 pathway, in which Toll-like receptor 4 is involved, are thought to be involved in cardiac hypertrophy [55]. *Creb1* encodes cAMP responsive element binding protein 1, a member of the leucine zipper family of cAMP-responsive element binding proteins. A study showed that *Creb1* can inhibit ferroptosis by binding to the GPX4 promoter region and increasing GPX4 activity to inhibit lipid peroxidation [56]. In addition, a study suggested that the protein expression of CREB is significantly reduced in the hearts of patients with heart failure, similar to what we observed in HFpEF mice [57]. *Egr1* is mainly involved in the regulation of gene expression and hormone synthesis processes [58]. In the heart, *Egr1* has been shown to be associated with myocardial growth [59]. We observed downregulation of EGR expression in HFpEF mice, which was reversed after the use of a ferroptosis inhibitor. However, one report suggests that *Egr1* is significantly associated with right ventricular hypertrophy due to pulmonary hypertension [60]. The role of *Egr1* in the development of HFpEF still needs further validation. *Hmox1* encodes heme oxygenase, a key rate-limiting enzyme that catalyzes the production of iron ions from heme. Unlike other screened hub DEGs, Hmox1 has been more thoroughly investigated to further contribute to myocardial hypertrophy and myocardial injury through activation of ferroptosis [9, 61]. However, the role of *Hmox1* in HFpEF remains unresolved. *Cd44* is a single transmembrane

glycoprotein involved in several biological processes [62]. *Cd44* induces inflammation in the body circulation, myocardial fibrosis and cardiac hypertrophy through binding to its ligand hyaluronic acid [63]. *Vdr* encodes the vitamin D receptor. A study showed that myocardial hypertrophy occurs in *Vdr* knockout mice due to activation of the angiotensin system [64]. However, a previous study suggested that activation of zebrafish cardiac *Vdr* leads to increased proliferation and regeneration of the heart [65]. *Lcn2* encodes lipocalcin 2 and can reduce inflammation by binding to iron carriers [66]. Several studies suggest that LCN2 protein is a risk factor for atherosclerosis and myocardial ischemic injury [67–69]. A recent study showed that the protein level of LCN2 in the heart is strongly associated with nonphysiological enlargement of the heart [70]. This is consistent with our observation of increased Lcn2 expression in the hearts of HFpEF mice, but whether *Lcn2* is involved in HFpEF through ferroptosis requires further verification. *Tfap2a* encodes a transcription factor, activator protein 2 (AP-2), which is primarily associated with the regulation of gene transcription [71]. Currently, there are still too few studies on *Tfap2a* in cardiac diseases. FU Muller et al. found that AP-2 expression was increased in the hearts of patients with idiopathic dilated cardiomyopathy and that AP-2 was associated with cardiomyocyte apoptosis in rats [72]. This is different from our finding of reduced *Tfap2a* transcript levels in HFpEF mice, and we speculate that this may be due to the large differences in pathophysiologic mechanisms between HFpEF and idiopathic dilated cardiomyopathy.

We have also experimentally demonstrated that aberrant activation of ferroptosis does exist in the hearts of HFpEF mice and have found a remission of the HFpEF phenotype and altered expression levels of pivotal genes after ferroptosis is inhibited. One thing to point out is that in the animal experiments section, our HFpEF mouse model remained consistent with the dataset, and both were fed a high-fat diet and L+NAME for 5 weeks. However, in the HFpEF+Fer-1, HFpEF+DFP and HFpEF+Veh groups, we took into account the normal clinical course of treatment, i.e., treatment is usually administered after diagnosis, so we continued to feed a high-fat diet and L-NAME while intraperitoneal injection of Fer-1 or DFP was given for 2 weeks after successful HFpEF modeling.

It is important to note that the mechanism of HFpEF occurrence has been shown to be significantly related to lipid metabolism [34]. A recent human plasma and endomyocardial metabolomics study reported that multiple metabolites of fatty acid oxidation was markedly lower in the myocardium of HFpEF patients, and the expression of genes related to fatty acid metabolism was also reduced in the HFpEF group [73]. In another study,

accumulation of epicardial adipose tissue was observed, which was associated with worse hemodynamic and metabolic profiles, as well as survival, in HFpEF patients [74]. Lipid accumulation induces cardiac lipotoxicity and subsequent myocardial dysfunction through multiple pathways, including increasing the generation of ROS [75].

Nevertheless, this study still has some limitations. First, our study is based on a public dataset, and the results obtained are largely exploratory and may differ somewhat from the actual results. At the same time, the dataset we downloaded from FerroDb does not summarize all ferroptosis-related genes and may contain some degree of omission. Second, due to the small number of studies on HFpEF, we only obtained a dataset from the transcriptome analysis of cardiac tissues from HFpEF mice, and the results obtained from the analysis may not be well represented. More regrettably, we did not obtain and analyze a transcriptome dataset from humans. We were also unable to obtain cardiac tissues from patients for further validation because of experimental ethical reasons. Although human genes and mouse genes share a certain degree of homology, there are still major differences in structure and function. HFpEF as a systemic inflammatory disease, we have not explored the role that other tissues such as liver and skeletal muscle play in the progression of HFpEF and the contribution of inflammation and immunity in HFpEF. It is worth noting that the specific metabolic mechanisms involved in the involvement of ferroptosis in the development of HFpEF were not further explored in our study, and whether these metabolic alterations regulate ferroptosis and HFpEF warrants a more comprehensive study in the future.

Conclusion

In conclusion, we obtained common hub DEGs associated with ferroptosis and HFpEF by bioinformatics analysis. We also verified the corresponding changes in the hub DEGs by RT-qPCR in the hearts of HFpEF mice and in the hearts after the use of ferroptosis inhibitors, suggesting that these hub DEGs may be involved in the development of HFpEF through ferroptosis. Eleven hub DEGs could be potential targets of drug action for the treatment of HFpEF, but further detailed experimental validation is still needed.

Abbreviations

ATF4	Activating transcription factor 4
BP	Biological process
CC	Cellular component
DEGs	Differentially expressed genes
DFP	Deferiprone
DHE	Dihydroethidium
FerrDb	Ferroptosis database
Fer-1	Ferrostatin-1
GO	Gene ontology

Xiong *et al. Journal of Translational Medicine*   (2024) 22:199

Page 15 of 17

GPX4	Glutathione peroxidase 4
GSH	Glutathione
HFD	High-fat diet
HFpEF	Heart failure with preserved ejection fraction
HFrEF	Heart failure with reduced ejection fraction
KEGG	Kyoto Encyclopedia of Genes and Genomes
L-NAME	N^ω-Nitro-L-arginine methyl ester
LVDd	Left ventricular internal diameter at diastole
LVDs	Left ventricular internal diameter at systole
LVPWd	Left ventricular posterior wall thickness at diastole
LVSd	Interventricular septal end diastole
MDA	Malondialdehyde
MF	Molecular function
MT	Masson's trichrome
NCBI	National Center for Biotechnology Information
NRF2	Nuclear factor red lineage 2-related factor 2
PPAR	Peroxisome proliferator-activated receptors
PPI	Protein–protein interaction
ROS	Reactive oxygen species
RT-qPCR	Real-time quantitative polymerase chain reaction
SOD	Superoxide dismutase
WGA	Wheat germ agglutinin

Supplementary Information

The online version contains supplementary material available at https://doi.org/10.1186/s12967-023-04734-y.

Additional file 1: Table S1. Primer sequences for RT qPCR.

Additional file 2: Table S2. Differentially expressed genes involved in HFpEF samples.

Additional file 3: Figure S1. Top five KEGG pathway enrichment results in GSE180065.

Additional file 4: Table S3. GO enrichment analysis of DEGs from GSE180065.

Additional file 5: Table S4. KEGG pathway enrichment analysis of DEGs from GSE180065.

Additional file 6: Table S5. GO enrichment analysis of ferroptosis-related DEGs.

Additional file 7: Table S6. KEGG pathway enrichment analysis of ferroptosis-related DEGs.

Additional file 8: Figure S2. Additional material related to Figure 3. **A** LVPWd, n = 5 mice per group. **B** LVDd, n = 5 mice per group. **C** LVDs, n = 5 mice per group. **D** LVSd, n = 5 mice per group. **E** Area under the curve of the intraperitoneal glucose tolerance test experiment, n = 5 mice per group. **F** Representative images of immunohistochemical staining showing macrophage infiltration in the heart tissue, n = 5 mice per group. Statistical significance was calculated by Student's t test; *P < 0.05, **P < 0.01, ***P < 0.001.

Additional file 9: Figure S3. Fer-1 and DFP inhibit intramyocardial ferroptosis and ameliorate the HFpEF phenotype. **A** Percentage of Prussian blue-stained positive cells, n = 5 mice per group. **B** Average protein levels of SLC7A11, GPX4, NRF2 and ATF4 in mouse heart tissue, n = 5 mice per group. **C** LVPWd, n = 5 mice per group. **D** LVDd, n = 5 mice per group. **E** LVDs, n = 5 mice per group. **F** LVSd, n = 5 mice per group. **(G)** Area under the curve of the intraperitoneal glucose tolerance test experiment, n = 5 mice per group. **H** Representative images of immunohistochemical staining showing macrophage infiltration in the heart tissue, n = 5 mice per group. Statistical significance was calculated by one-way ANOVA; *P < 0.05, **P < 0.01, ***P < 0.001.

 Availability of data and materials
The datasets analyzed during the current study are available in the GEO database (https://www.ncbi.nlm.nih.gov/geo/) and FerrDb (http://www.zhounan.org/ferrdb/).

Declarations

Ethics approval and consent to participate
All animal experiments were performed with the approval of the Institutional Animal Care and Use Committee of the West China Hospital, Sichuan University, China (Protocol# 20220926004).

Consent for publication
Not applicable.

Competing interests
The authors declare that they have no competing interests.

Author details
[1]Department of Anesthesiology, National-Local Joint Engineering Research Centre of Translational Medicine of Anesthesiology, West China Hospital, Sichuan University, No 37 Wainan Guoxue Road, Sichuan 610041, China. [2]Laboratory of Mitochondria and Metabolism, West China Hospital, Sichuan University, Sichuan 610041, China. [3]Department of Anesthesiology, West China Second Hospital of Sichuan University, Chengdu 610041, Sichuan, China. [4]Key Laboratory of Birth Defects and Related Diseases of Women and Children (Sichuan University), Ministry of Education, Sichuan University, Chengdu 610041, Sichuan, China. [5]Department of Gastroenterology, Chengdu Fifth People's Hospital, No. 33 Mashi Street, Chengdu 611130, Sichuan, China. [6]Nursing Key Laboratory of Sichuan Province, West China Hospital, Sichuan University, No 37 Wainan Guoxue Road, Chengdu 610041, Sichuan, China.

Published online: 24 February 2024

References

1. Borlaug BA. Evaluation and management of heart failure with preserved ejection fraction. Nat Rev Cardiol. 2020;17:559–73. https://doi.org/10.1038/s41569-020-0363-2.
2. Redfield MM. Heart failure with preserved ejection fraction. N Engl J Med. 2016;375:1868–77. https://doi.org/10.1056/NEJMcp1511175.
3. McHugh K, et al. Heart failure with preserved ejection fraction and diabetes: JACC state-of-the-art review. J Am Coll Cardiol. 2019;73:602–11. https://doi.org/10.1016/j.jacc.2018.11.033.
4. Anker SD, et al. Empagliflozin in heart failure with a preserved ejection fraction. N Engl J Med. 2021;385:1451–61. https://doi.org/10.1056/NEJMoa2107038.
5. Omote K, Verbrugge FH, Borlaug BA. Heart failure with preserved ejection fraction: mechanisms and treatment strategies. Annu Rev Med. 2022;73:321–37. https://doi.org/10.1146/annurev-med-042220-022745.
6. Dixon SJ, et al. Ferroptosis: an iron-dependent form of nonapoptotic cell death. Cell. 2012;149:1060–72. https://doi.org/10.1016/j.cell.2012.03.042.

Xiong *et al. Journal of Translational Medicine*   (2024) 22:199

Page 16 of 17

7. Jiang X, Stockwell BR, Conrad M. Ferroptosis: mechanisms, biology and role in disease. Nat Rev Mol Cell Biol. 2021;22:266–82. https://doi.org/10.1038/s41580-020-00324-8.

8. Stockwell BR, et al. Ferroptosis: a regulated cell death nexus linking metabolism, redox biology, and disease. Cell. 2017;171:273–85. https://doi.org/10.1016/j.cell.2017.09.021.

9. Fang X, et al. Ferroptosis as a target for protection against cardiomyopathy. Proc Natl Acad Sci USA. 2019;116:2672–80. https://doi.org/10.1073/pnas.1821022116.

10. Zheng Y, et al. Novel lncRNA-miRNA-mRNA competing endogenous RNA triple networks associated programmed cell death in heart failure. Front Cardiovasc Med. 2021;8: 747449. https://doi.org/10.3389/fcvm.2021.747449.

11. Friedmann Angeli JP, et al. Inactivation of the ferroptosis regulator Gpx4 triggers acute renal failure in mice. Nat Cell Biol. 2014;16:1180–91. https://doi.org/10.1038/ncb3064.

12. Lei G, Zhuang L, Gan B. Targeting ferroptosis as a vulnerability in cancer. Nat Rev Cancer. 2022;22:381–96. https://doi.org/10.1038/s41568-022-00459-0.

13. Chen X, Kang R, Kroemer G, Tang D. Broadening horizons: the role of ferroptosis in cancer. Nat Rev Clin Oncol. 2021;18:280–96. https://doi.org/10.1038/s41571-020-00462-0.

14. Wang J, et al. Pyroptosis and ferroptosis induced by mixed lineage kinase 3 (MLK3) signaling in cardiomyocytes are essential for myocardial fibrosis in response to pressure overload. Cell Death Dis. 2020;11:574. https://doi.org/10.1038/s41419-020-02777-3.

15. Ning D, et al. Atorvastatin treatment ameliorates cardiac function and remodeling induced by isoproterenol attack through mitigation of ferroptosis. Biochem Biophys Res Commun. 2021;574:39–47. https://doi.org/10.1016/j.bbrc.2021.08.017.

16. Hahn VS, et al. Myocardial gene expression signatures in human heart failure with preserved ejection fraction. Circulation. 2021;143:120–34. https://doi.org/10.1161/CIRCULATIONAHA.120.050498.

17. Tang B, et al. Targeted xCT-mediated ferroptosis and protumoral polarization of macrophages is effective against HCC and enhances the efficacy of the anti-PD-1/L1 response. Adv Sci. 2023;10:e2203973. https://doi.org/10.1002/advs.202203973.

18. Xing G, et al. PPARalpha alleviates iron overload-induced ferroptosis in mouse liver. EMBO Rep. 2022;23:e52280. https://doi.org/10.15252/embr.202052280.

19. Schiattarella GG, et al. Nitrosative stress drives heart failure with preserved ejection fraction. Nature. 2019;568:351–6. https://doi.org/10.1038/s41586-019-1100-z.

20. Zhang Z, et al. Elabela alleviates ferroptosis, myocardial remodeling, fibrosis and heart dysfunction in hypertensive mice by modulating the IL-6/STAT3/GPX4 signaling. Free Radic Biol Med. 2022;181:130–42. https://doi.org/10.1016/j.freeradbiomed.2022.01.020.

21. Zheng H, Shi L, Tong C, Liu Y, Hou M. circSnx12 is involved in ferroptosis during heart failure by targeting miR-224-5p. Front Cardiovasc Med. 2021;8: 656093. https://doi.org/10.3389/fcvm.2021.656093.

22. Yang WS, et al. Regulation of ferroptotic cancer cell death by GPX4. Cell. 2014;156:317–31. https://doi.org/10.1016/j.cell.2013.12.010.

23. Tang D, Chen X, Kang R, Kroemer G. Ferroptosis: molecular mechanisms and health implications. Cell Res. 2021;31:107–25. https://doi.org/10.1038/s41422-020-00441-1.

24. Mao C, et al. DHODH-mediated ferroptosis defence is a targetable vulnerability in cancer. Nature. 2021;593:586–90. https://doi.org/10.1038/s41586-021-03539-7.

25. Ahola S, et al. OMA1-mediated integrated stress response protects against ferroptosis in mitochondrial cardiomyopathy. Cell Metab. 2022;34:1875–91.e1877. https://doi.org/10.1016/j.cmet.2022.08.017.

26. Jiang L, et al. Ferroptosis as a p53-mediated activity during tumour suppression. Nature. 2015;520:57–62. https://doi.org/10.1038/nature14344.

27. Fang X, Ardehali H, Min J, Wang F. The molecular and metabolic landscape of iron and ferroptosis in cardiovascular disease. Nat Rev Cardiol. 2023;20:7–23. https://doi.org/10.1038/s41569-022-00735-4.

28. Wang Y, et al. PRMT4 promotes ferroptosis to aggravate doxorubicin-induced cardiomyopathy via inhibition of the Nrf2/GPX4 pathway. Cell Death Differ. 2022;29:1982–95. https://doi.org/10.1038/s41418-022-00990-5.

29. He F, et al. ATF4 suppresses hepatocarcinogenesis by inducing SLC7A11 (xCT) to block stress-related ferroptosis. J Hepatol. 2023;79:362–77. https://doi.org/10.1016/j.jhep.2023.03.016.

30. Kwiatkowski JL. Current recommendations for chelation for transfusion-dependent thalassemia. Ann N Y Acad Sci. 2016;1368:107–14. https://doi.org/10.1111/nyas.13088.

31. Redfield MM, Borlaug BA. Heart failure with preserved ejection fraction: a review. JAMA. 2023;329:827–38. https://doi.org/10.1001/jama.2023.2020.

32. Schiattarella GG, Rodolico D, Hill JA. Metabolic inflammation in heart failure with preserved ejection fraction. Cardiovasc Res. 2021;117:423–34. https://doi.org/10.1093/cvr/cvaa217.

33. Liu J, et al. Epicardial adipose tissue density is a better predictor of cardio-metabolic risk in HFpEF patients: a prospective cohort study. Cardiovasc Diabetol. 2023;22:45. https://doi.org/10.1186/s12933-023-01778-8.

34. Capone F, et al. Cardiac metabolism in HFpEF: from fuel to signalling. Cardiovasc Res. 2023;118:3556–75. https://doi.org/10.1093/cvr/cvac166.

35. Fang X, et al. Loss of cardiac ferritin H facilitates cardiomyopathy via Slc7a11-mediated ferroptosis. Circ Res. 2020;127:486–501. https://doi.org/10.1161/CIRCRESAHA.120.316509.

36. Green DR. The coming decade of cell death research: five riddles. Cell. 2019;177:1094–107. https://doi.org/10.1016/j.cell.2019.04.024.

37. Liao P, et al. CD8(+) T cells and fatty acids orchestrate tumor ferroptosis and immunity via ACSL4. Cancer Cell. 2022;40:365-378.e366. https://doi.org/10.1016/j.ccell.2022.02.003.

38. Gao W, Wang X, Zhou Y, Wang X, Yu Y. Autophagy, ferroptosis, pyroptosis, and necroptosis in tumor immunotherapy. Signal Transduct Target Ther. 2022;7:196. https://doi.org/10.1038/s41392-022-01046-3.

39. Sanders-van Wijk S, et al. Proteomic evaluation of the comorbidity-inflammation paradigm in heart failure with preserved ejection fraction: results from the PROMIS-HFpEF study. Circulation. 2020;142:2029–44. https://doi.org/10.1161/CIRCULATIONAHA.120.045810.

40. Kolijn D, et al. Empagliflozin improves endothelial and cardiomyocyte function in human heart failure with preserved ejection fraction via reduced pro-inflammatory-oxidative pathways and protein kinase galpha oxidation. Cardiovasc Res. 2021;117:495–507. https://doi.org/10.1093/cvr/cvaa123.

41. Franssen C, et al. Myocardial microvascular inflammatory endothelial activation in heart failure with preserved ejection fraction. JACC Heart Fail. 2016;4:312–24. https://doi.org/10.1016/j.jchf.2015.10.007.

42. Zhang N, et al. CXCR4-dependent macrophage-to-fibroblast signaling contributes to cardiac diastolic dysfunction in heart failure with preserved ejection fraction. Int J Biol Sci. 2022;18:1271–87. https://doi.org/10.7150/ijbs.65802.

43. Deng Y, et al. Targeting mitochondria-inflammation circuit by beta-hydroxybutyrate mitigates HFpEF. Circ Res. 2021;128:232–45. https://doi.org/10.1161/CIRCRESAHA.120.317933.

44. Chirinos JA, et al. Multiple plasma biomarkers for risk stratification in patients with heart failure and preserved ejection fraction. J Am Coll Cardiol. 2020;75:1281–95. https://doi.org/10.1016/j.jacc.2019.12.069.

45. Zhang B, et al. Oleic acid alleviates LPS-induced acute kidney injury by restraining inflammation and oxidative stress via the Ras/MAPKs/PPAR-gamma signaling pathway. Phytomedicine. 2022;94: 153818. https://doi.org/10.1016/j.phymed.2021.153818.

46. Wu X, et al. SIRT6 mitigates heart failure with preserved ejection fraction in diabetes. Circ Res. 2022;131:926–43. https://doi.org/10.1161/CIRCRESAHA.121.318988.

47. Kamimura D, Uchino K, Ishigami T, Hall ME, Umemura S. Activation of peroxisome proliferator-activated receptor gamma prevents development of heart failure with preserved ejection fraction; inhibition of wnt-beta-catenin signaling as a possible mechanism. J Cardiovasc Pharmacol. 2016;68:155–61. https://doi.org/10.1097/FJC.0000000000000397.

48. Janani C, Kumari BR. PPAR gamma gene—a review. Diabetes Metab Syndr. 2015;9:46–50. https://doi.org/10.1016/j.dsx.2014.09.015.

49. Chen H, et al. PPAR-gamma signaling in nonalcoholic fatty liver disease: pathogenesis and therapeutic targets. Pharmacol Ther. 2023;245: 108391. https://doi.org/10.1016/j.pharmthera.2023.108391.

50. Legchenko E, et al. PPARgamma agonist pioglitazone reverses pulmonary hypertension and prevents right heart failure via fatty acid oxidation. Sci Transl Med. 2018. https://doi.org/10.1126/scitranslmed.aao0303.

51. Lopez-Castejon G, Brough D. Understanding the mechanism of IL-1beta secretion. Cytokine Growth Factor Rev. 2011;22:189–95. https://doi.org/10.1016/j.cytogfr.2011.10.001.

52. Huang Y, Xu W, Zhou R. NLRP3 inflammasome activation and cell death. Cell Mol Immunol. 2021;18:2114–27. https://doi.org/10.1038/s41423-021-00740-6.

53. Higashikuni Y, et al. NLRP3 inflammasome activation through heart-brain interaction initiates cardiac inflammation and hypertrophy during pressure overload. Circulation. 2023;147:338–55. https://doi.org/10.1161/CIRCULATIONAHA.122.060860.

54. Regueira T, et al. Hypoxia inducible factor-1 alpha induction by tumour necrosis factor-alpha, but not by toll-like receptor agonists, modulates cellular respiration in cultured human hepatocytes. Liver Int. 2009;29:1582–92. https://doi.org/10.1111/j.1478-3231.2009.02109.x.

55. Li Y, et al. Modified citrus pectin prevents isoproterenol-induced cardiac hypertrophy associated with p38 signalling and TLR4/JAK/STAT3 pathway. Biomed Pharmacother. 2021;143: 112178. https://doi.org/10.1016/j.biopha.2021.112178.

56. Wang Z, et al. CREB stimulates GPX4 transcription to inhibit ferroptosis in lung adenocarcinoma. Oncol Rep. 2021;45:45. https://doi.org/10.3892/or.2021.8039.

57. Wu S, et al. Binding of FUN14 domain containing 1 with inositol 1,4,5-trisphosphate receptor in mitochondria-associated endoplasmic reticulum membranes maintains mitochondrial dynamics and function in hearts in vivo. Circulation. 2017;136:2248–66. https://doi.org/10.1161/CIRCULATIONAHA.117.030235.

58. Chen JW, et al. Transient upregulation of EGR1 signaling enhances kidney repair by activating SOX9(+) renal tubular cells. Theranostics. 2022;12:5434–50. https://doi.org/10.7150/thno.73426.

59. Maass A, Suppl C, et al. Hormonal induction of an immediate-early gene response in myogenic cell lines—a paradigm for heart growth. Eur Heart J. 1995;16:12–4. https://doi.org/10.1093/eurheartj/16.suppl_c.12.

60. Laggner M, et al. EGR1 is implicated in right ventricular cardiac remodeling associated with pulmonary hypertension. Biology. 2022. https://doi.org/10.3390/biology11050677.

61. Allwood MA, et al. Heme oxygenase-1 overexpression exacerbates heart failure with aging and pressure overload but is protective against isoproterenol-induced cardiomyopathy in mice. Cardiovasc Pathol. 2014;23:231–7. https://doi.org/10.1016/j.carpath.2014.03.007.

62. Chen C, Zhao S, Karnad A, Freeman JW. The biology and role of CD44 in cancer progression: therapeutic implications. J Hematol Oncol. 2018;11:64. https://doi.org/10.1186/s13045-018-0605-5.

63. Suleiman M, Abdulrahman N, Yalcin H, Mraiche F. The role of CD44, hyaluronan and NHE1 in cardiac remodeling. Life Sci. 2018;209:197–201. https://doi.org/10.1016/j.lfs.2018.08.009.

64. Xiang W, et al. Cardiac hypertrophy in vitamin D receptor knockout mice: role of the systemic and cardiac renin-angiotensin systems. Am J Physiol Endocrinol Metab. 2005;288:E125–32. https://doi.org/10.1152/ajpendo.00224.2004.

65. Han Y, et al. Vitamin D stimulates cardiomyocyte proliferation and controls organ size and regeneration in Zebrafish. Dev Cell. 2019;48:853–63. e855. https://doi.org/10.1016/j.devcel.2019.01.001.

66. Yang HH, et al. Lipocalin family proteins and their diverse roles in cardiovascular disease. Pharmacol Ther. 2023;244: 108385. https://doi.org/10.1016/j.pharmthera.2023.108385.

67. Huang G, et al. Associations between retinol-binding protein 4 and cardiometabolic risk factors and subclinical atherosclerosis in recently postmenopausal women: cross-sectional analyses from the KEEPS study. Cardiovasc Diabetol. 2012;11:52. https://doi.org/10.1186/1475-2840-11-52.

68. Cheng JM, et al. Circulating osteoglycin and NGAL/MMP9 complex concentrations predict 1-year major adverse cardiovascular events after coronary angiography. Arterioscler Thromb Vasc Biol. 2014;34:1078–84. https://doi.org/10.1161/ATVBAHA.114.303486.

69. Shibata K, et al. Lipocalin-2 exerts pro-atherosclerotic effects as evidenced by in vitro and in vivo experiments. Heart Vessels. 2020;35:1012–24. https://doi.org/10.1007/s00380-020-01556-6.

70. Marques FZ, et al. Experimental and human evidence for lipocalin-2 (neutrophil gelatinase-associated lipocalin [NGAL]) in the development of cardiac hypertrophy and heart failure. J Am Heart Assoc. 2017. https://doi.org/10.1161/JAHA.117.005971.

71. Yuanhua L, et al. TFAP2A induced KRT16 as an oncogene in lung adenocarcinoma via EMT. Int J Biol Sci. 2019;15:1419–28. https://doi.org/10.7150/ijbs.34076.

72. Muller FU, et al. Transcription factor AP-2alpha triggers apoptosis in cardiac myocytes. Cell Death Differ. 2004;11:485–93. https://doi.org/10.1038/sj.cdd.4401383.

73. Hahn VS, et al. Myocardial metabolomics of human heart failure with preserved ejection fraction. Circulation. 2023;147:1147–61. https://doi.org/10.1161/CIRCULATIONAHA.122.061846.

74. Pugliese NR, et al. Impact of epicardial adipose tissue on cardiovascular haemodynamics, metabolic profile, and prognosis in heart failure. Eur J Heart Fail. 2021;23:1858–71. https://doi.org/10.1002/ejhf.2337.

75. Schulze PC, Drosatos K, Goldberg IJ. Lipid use and misuse by the heart. Circ Res. 2016;118:1736–51. https://doi.org/10.1161/CIRCRESAHA.116.306842.

Publisher's Note